Experimental validation of the modified Avrami model for non-isothermal crystallization conditions

Ricky Sze Ho Lam and Michael A. Rogers*

Received 10th August 2010, Accepted 15th September 2010
DOI: 10.1039/c0ce00523a

The modified Avrami model was found to accurately predict the induction time, maximum phase volume and dimensionality of crystal growth for stearic acid containing molecules when the experimental method employed measures as a function of phase volume. Four methods were examined to validate the model including: Fourier transformed infrared spectroscopy (FT-IR), differential scanning calorimetry (DSC), small deformation rheology and polarized light microscopy (PLM). PLM and FT-IR were able to detect the nucleation event prior to DSC and rheology. FT-IR and PLM provided the most accurate data due to the similarities between the experimental and fitted induction times (x_0), maximal phase change (y_{max}) and the Avrami exponent (n). Further, the Avrami exponent, obtained from FT-IR, was sensitive to both the mode of nucleation and the dimensionality of crystal growth. Therefore, the apparent rate constants (k_{app}) obtained by FT-IR and PLM are useful in providing further insights into the kinetics of non-isothermal crystallization. The calculated apparent rate constants suggest a diffusion limited crystallization at slow cooling rates (*i.e.*, below 5–7 °C min^{-1}) and at cooling rates greater than 5–7 °C min^{-1}, the incorporation of the gelator molecules onto the crystal lattice becomes limited by the reaction rate constant.

Introduction

Dimensionality of crystal growth is essential in determining the physical properties of crystalline materials.[1] The dimensionality of crystal growth is represented by the number of axes of the crystal in which growth takes place (Fig. 1). For 1-dimensional crystals, growth occurs in one axis, for 2-dimensional crystals growth occurs in two axes forming a plane and for 3-dimensional crystals growth occurs on all 3 axes forming a sphere. Emphasis has traditionally focused on high-dimensionality crystals in fields such as oxide and phosphate inorganic chemistry,[2] polymer chemistry[3] and lipid chemistry.[4] However, current advances in low-dimensionality crystals including nanowires, nanotubes and nanoplatelets are becoming crucial for numerous practical applications propelling these technologies to the forefront of crystal physics and chemistry. Low-dimensionality crystals are revolutionizing lipid chemistry,[5–9] ceramics,[10] and chemo-responsive gels.[11] To further the applications of low-dimensionality crystals not only a practical understanding is required but also a fundamental understanding into their nucleation and crystal growth mechanisms is essential.[12]

Nucleation events result in the formation of a new phase from the 'mother' state *via* the formation of a three-dimensional spherical cluster or a "crystal embryo". The cluster forms, as the solution is cooled below the melting temperature, resulting in a super-saturated state causing molecules to microscopically or macroscopically phase separate.[13] "Crystal embryos" are spherical minimizing the surface free energy (*i.e.*, the major energy barrier needed to be overcome during crystallization) of the interface between the new phase and the previously existing phase. A meta-stable region exists because Brownian forces disrupt the formation of the crystal embryo while the formation of non-covalent interactions stabilizes the embryo. At elevated temperatures the Brownian forces exceed the non-covalent forces and the embryo is unstable. At lower temperatures, the non-covalent forces exceed the Brownian forces and the nuclei are stable. Depending on the cooling profile the mode of nucleation may be instantaneous (*i.e.*, all nuclei form at once) or sporadic (*i.e.*, nuclei form as a function of time). Following nucleation, the crystal grows either as three-dimensional spheres, two-dimensional plates or discs, or one-dimensional fibers.

Crystal physics has long been concerned with not only the rate of crystal growth but also the dimensionality of how materials assemble during crystallization.[14–16] For practical applications, the effect of non-isothermal crystallization conditions on the microstructure and macrostructure is of utmost importance.[17,18] The kinetics of a phase change is frequently modeled using the Avrami equation where it is assumed that the number and size of the crystals are functions of time and temperature.[14] The Avrami model has previously been derived from Fick's first law of diffusion.[4]

However, in industrial applications, crystallization typically occurs under non-isothermal cooling conditions (*i.e.*, the temperature changes as the material crystallizes) inducing different physical properties. The nucleation and crystallization rate change as a function of time because heat and mass transfer conditions evolved as temperature is decreased. Nucleation behavior is of great importance due to the effect on structural features including crystal size, crystal morphology and the spatial distribution of the crystalline mass.[7,19,20] Therefore, the model for isothermal cooling has been adapted for non-isothermal conditions and takes the following form:[17,18]

$$\frac{Y_s}{Y_{max}} = 1 - e^{-k_{app}(x-x_0)^n} \quad (1)$$

Department of Food and Bioproduct Sciences, University of Saskatchewan, Saskatoon, SK, Canada S7N5A8. E-mail: michael.rogers@usask.ca; Fax: +1 306 966 8898; Tel: +1 306 966 5028

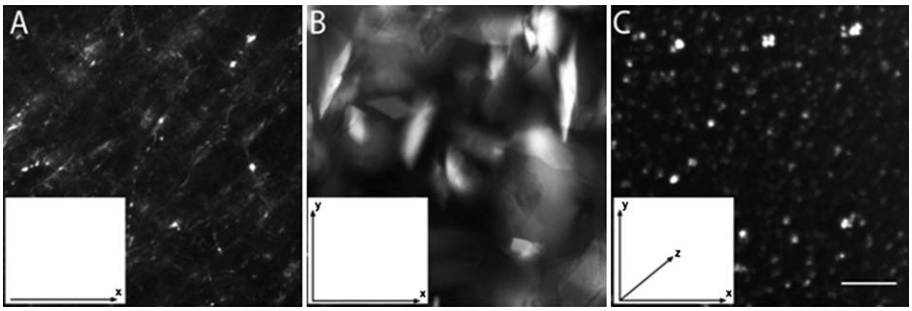

Fig. 1 Polarized light micrographs of 1D fibers (12-hydroxystearic acid) (A), 2D platelets (stearic acid) (B), and 3D spherulite (trihydroxystearin) (C) with their respective axes of crystal growth represented by x, y and z. Bar = 5 μm.

where k_{app} is the apparent rate constant, x is the time and x_0 is the induction time, n is the Avrami exponent representing both the dimensionality of growth and mode of nucleation. The Avrami exponent (n) is a function of both the dimensionality of crystal growth as well as the mode of nucleation (*i.e.*, sporadic or instantaneous).[21] Although numerous reports have been presented using the non-isothermal Avrami model there has yet to be a systematic study evaluating the applicability of this model or the experimental techniques used to measure the change in crystal phase volume. Not all techniques used to measure crystal phase volume are applicable such as turbidity because crystal growth progresses beyond the y_{max} of the light scattering.[22]

Two other approaches to modeling crystal growth under non-isothermal cooling conditions have been reported.[23–25] Rousset developed the finite element method which utilizes the isothermal time, temperature and transformation diagrams (FEM-TTT).[24] Isothermal time–temperature–transformation (TTT) diagrams are crystallization data collected under isothermal cooling conditions at different temperatures.[24] FEM-TTT utilizes isothermal data which are applied to non-isothermal cooling conditions.[24] The thermal path for crystallization under non-isothermal conditions is obtained and splits into small segments which are analyzed isothermally.[24] Each segment is assigned a corresponding isothermal temperature whereby data from TTT diagrams are used to extrapolate the relative amount of phase transition undergone at that time interval.[24] A series of these time segments are analyzed isothermally and pieced together to determine the path of the phase transition experienced by the sample under non-isothermal cooling conditions.[24]

An isoconversional method to model phase transition in lipids has also been reported where data are not fitted to a specific model.[23,25] The phase transition is captured and the first derivative is utilized to measure the change in the rate of the phase transition as the sample undergoes non-isothermal cooling conditions.[23,25] The FEM-TTT and the isoconversional methods both provide phase transition kinetics but provide no data on the mode of nucleation or the dimensionality of crystal growth. In these two models the kinetic data are determined experimentally and *via* the model which can be compared for accuracy; however, there are no alternative parameters to verify their accuracy. The modified Avrami model can utilize the Avrami exponent, which indicates the mode of nucleation and dimensionality of crystal growth, induction time, and the maximal crystal phase volume to verify the fit to the experimental data.

In this systematic study three stearic acid containing molecules were examined to assess the modified Avrami model. 12-Hydroxystearic acid (12HSA) crystallizes into 1-dimensional fibers (Fig. 1A).[6,7,17,18,20,26–30] This is due to the incorporation of 12HSA molecules *via* van der Waals interactions and hydrogen bonding.[31] Stearic acid (Fig. 1B) crystallizes into two-dimensional rhombic platelets.[9,32,33] Trihydroxystearin (Fig. 1C) forms 3-dimensional spherulitic crystals. In 2- and 3-D systems, growth occurs with the alignment of the alkane chains which maximizes the van der Waals interactions required for crystal growth among stearic acid and trihydroxystearin.[31,34] The purpose of this research is to experimentally validate the use of the modified Avrami equation under non-isothermal crystallization conditions.

Derivation of the modified Avrami model from Fick's first law of diffusion

Fick's first law of diffusion is:

$$\frac{\partial Q}{\partial t} = DA\left(\frac{\Delta C}{\Delta x}\right) \tag{2}$$

where $\partial Q/\partial t$ is the number of moles of material (Q) crystallized as a function of time (t), D is the diffusion coefficient, A is the area of diffusion and $\Delta C/\Delta x$ is the changing concentration of soluble material (C), which is the decrease due to crystallization, across a thickness (x) of boundary layer. If the mass of a crystal (Y_c) is proportional to the number of moles and the molecular weight of the crystallizing molecules (MW), then diffusion across the boundary layer onto the crystal surface may be rewritten as:

$$\frac{\partial Y_c}{\partial t} = \frac{\partial Q}{\partial t}\mathrm{MW} \text{ or } \frac{\partial Y_c}{\partial t} = DA\left(\frac{\Delta C}{\Delta x}\right)\mathrm{MW} \tag{3}$$

The rate of mass deposition onto a crystal surface can be expressed as a rate constant for crystal growth (k_g). This parameter (k_g) is typically used in describing crystal growth and accounts for the two steps required for an increase in crystalline mass: the diffusion of the molecule to the crystal surface (D) across a distance (Δx) and the rate of incorporation of the molecule into the crystalline surface (κ). Hence k_g takes the following form:

$$k_g = \left(\frac{1}{D} + \frac{1}{\kappa}\right)^{-1} \Delta x^{-1} \tag{4}$$

and

$$(c - c^*) = \mathrm{MW}\Delta C \tag{5}$$

where c is the concentration of the supersaturated material and c^* is the equilibrium saturation concentration of the material per unit volume. Substituting eqn (4) and (5) into eqn (3) attains the following relationship:

$$\frac{\partial Y_c}{\partial t} = k_g A(c - c^*) \tag{6}$$

Eqn (5) may be rewritten since the mass of total solids (Y_s) is a function of the number of crystals (N) and the mass of the crystals (Y_c) assuming that the crystals are homogenous in nature:

$$\frac{\partial Y_s}{\partial t} = Nk_g A(c - c^*) \text{while } (c - c^*) = \frac{Y_{max} - Y_s}{V_t} \tag{7}$$

where ($Y_{max} - Y_s$) is the amount of uncrystallized material (Y_{max} is the total amount of solids at infinity and Y_s is the total solids at a given time) and V_t is the volume of the system. The number of crystals per unit volume (ρ) can be written as:

$$\rho = \frac{N}{V_t} \tag{8}$$

Substituting eqn (6) and (7) into eqn (5) followed by variable separation leads to the Avrami equation derived by Marangoni:[4]

$$\frac{\partial Y_s}{(Y_{max} - Y_s)} = k_g \rho A \partial t \tag{9}$$

At this point, eqn (8) represents instantaneous nucleation followed by crystal growth. In the case of sporadic nucleation, the number of crystals per unit volume (ρ) is a function of time (t) and the nucleation rate (j) and for sporadic nucleation eqn (8) is modified to become:

$$\frac{\partial Y_s}{(Y_{max} - Y_s)} = k_g jtA \partial t \tag{10}$$

Depending on the dimensionality of growth the area of the growing surface is represented by a sphere ($A = 4\pi r_{sphere}^2$ where A is the area and r is the radius), a platelet ($A = 4lh$ where l is the dimension of the growing plate and h is the non-propagating surface) or a fiber ($A = 2\pi r_{fiber}^2$ where r_{fiber} is the radius). For the radius of the sphere (r_{sphere}) it is assumed that it grows at a linear growth rate (g) as a function of time (t). Similarly, the growing dimension of the platelet (l) also has a linear growth rate (g) ($r = gt$ for a sphere or $l = gt$ for a platelet).

Hence the Avrami model, for each mode of nucleation and crystal growth shape, may be derived by substituting the growth area and the nucleation term. For illustration purposes the Avrami model for instantaneous nucleation with spherical growth (eqn (10)) is shown:

$$\frac{\partial Y_s}{(Y_{max} - Y_s)} = k_g \rho (4\pi g^2 t^2) \partial t \tag{11}$$

Eqn (10) may be integrated across the boundary condition $m_s = 0$ at time $t = 0$ and m_s at t:

$$\int_0^{ms} \frac{\partial Y_s}{(Y_{max} - Y_s)} = k_g \rho 4\pi g^2 \int_0^t t^2 \partial t \tag{12}$$

resulting in:

$$\ln\left(\frac{Y_s}{(Y_{max} - Y_s)}\right) = k_g \rho \frac{4}{3}\pi g^2 t^3 \tag{13}$$

which rearranges to:

$$\frac{Y_s}{Y_{max}} = 1 - e^{k_g \rho \frac{4}{3}\pi g^2 t^3} \tag{14}$$

hence for instantaneous nucleation and spherulitic crystal growth the Avrami equation is:

$$\frac{Y_s}{Y_{max}} = 1 - e^{Kt^3} \tag{15}$$

$$\text{where } K = k_g \rho \frac{4}{3}\pi g^2 \text{ and } n = 3.$$

Using the same logic in which eqn (14) was derived, the other possible forms of the Avrami model are presented (Table 1).

Materials and methods

12-Hydroxystearic acid (12HSA) (Nu-Chek Prep, Elysian, MN, USA), stearic acid (Sigma Aldrich, Oakville, ON) and trihydroxystearin (Nu-Chek Prep, Elysian, MN, USA) were purchased and used as received. 3% (w/w) of the stearic acid containing molecules were added to heavy mineral oil (Sigma Aldrich, Oakville, ON, CA) and were melted at 90 °C and held for 10 minutes to erase crystal memory. Cooling rates of 1–10 °C

Table 1 Possible forms of the Avrami model for the different modes of nucleation and their associated dimensionality of crystal growth (Marangoni, 2005)

Mode of nucleation	Dimensionality of crystal growth	Avrami equation	K	n
Instantaneous	Linear	$\frac{Y_s}{Y_{max}} = 1 - e^{Kt^1}$	$2\pi r^2 k_g j$	1
Sporadic	Linear	$\frac{Y_s}{Y_{max}} = 1 - e^{Kt^2}$	$\pi r^2 k_g j$	2
Instantaneous	Platelet	$\frac{Y_s}{Y_{max}} = 1 - e^{Kt^2}$	$2hk_g \rho g$	2
Sporadic	Platelet	$\frac{Y_s}{Y_{max}} = 1 - e^{Kt^3}$	$(4/3)hk_g jg$	3
Instantaneous	Spherulitic	$\frac{Y_s}{Y_{max}} = 1 - e^{Kt^3}$	$k_g \rho (4/3)\pi g^2$	3
Sporadic	Spherulitic	$\frac{Y_s}{Y_{max}} = 1 - e^{Kt^4}$	$jk_g \pi g^2$	4

min^{-1} at 1 °C increments and at 15 °C min^{-1} were applied to the samples when cooling from 90 °C to 30 °C.

Synchrotron Fourier transformed-infrared spectroscopy (FT-IR)

FT-IR was done at the Canadian Light Source (Saskatoon, SK, Canada) on the mid-IR beamline (beamline 01 B1-01, Canadian Light Source, Saskatoon, SK). The end station used is comprised of a Bruker Optics IFS66v/S interferometer coupled to a Hyperion 2000 IR microscope (Bruker Optics, Billerica, MA, USA). Light was focused on the system using a 15× magnification Schwarzschild condenser, collected by a 15× magnification Schwarzschild objective with the aperture set to a spot size of 40 μm by 40 μm and detected by a liquid nitrogen cooled narrowband MCT detector utilizing a 100 μm sensing element.

Spectra were collected at 32 scans per measurement from 690 to 7899 cm^{-1} at a spectral resolution of 4 cm^{-1}. The temperature controlled stage (LTS120 and PE94 temperature controller (Linkam, Surrey, UK)) was used to modify the cooling rate while collecting spectra on the FT-IR instrument.

A KBr-supported Ge multilayer beam splitter was used to measure spectra in the mid-infrared spectral region. Measurements were taken using the Opus 6.5 software (Bruker Optics, Billerica, MA). The systems were held in between two calcium fluoride optical windows (25 mm diameter, 2 mm thick) with a 15 μm Teflon spacer. Approximately 10 mg of the melted sample were held between the two calcium fluoride optical windows. The non-covalent hydrogen bonding was determined by analyzing for the carboxyl and hydroxyl peak at 1710 cm^{-1} and 3200 cm^{-1} respectively.[35] A spectrum was taken of the samples in the molten state at 90 °C where all subsequent spectra taken were compared to and the difference plotted. The peaks were analyzed by determining the area under these peaks using the Opus 6.5 Software (Bruker Optics, Billerica, MA). The areas for the two peaks were plotted as a function of time and fitted to the modified Avrami model. Due to restrictions such as the availability of time on the synchrotron, one replicate was performed for this analysis.

Differential scanning calorimetry

A Q2000 Differential Scanning Calorimeter (DSC) (TA Instruments, New Castle, Delaware, USA) was used to detect the evolution of heat during the exothermic phase transition. A 8–10 mg of sample was hermetically sealed in aluminium pans and thermograms were collected as the sample was cooled at different rates. TA analysis software (TA Instruments, New Castle, Delaware, USA) applied a running integral across the enthalpy

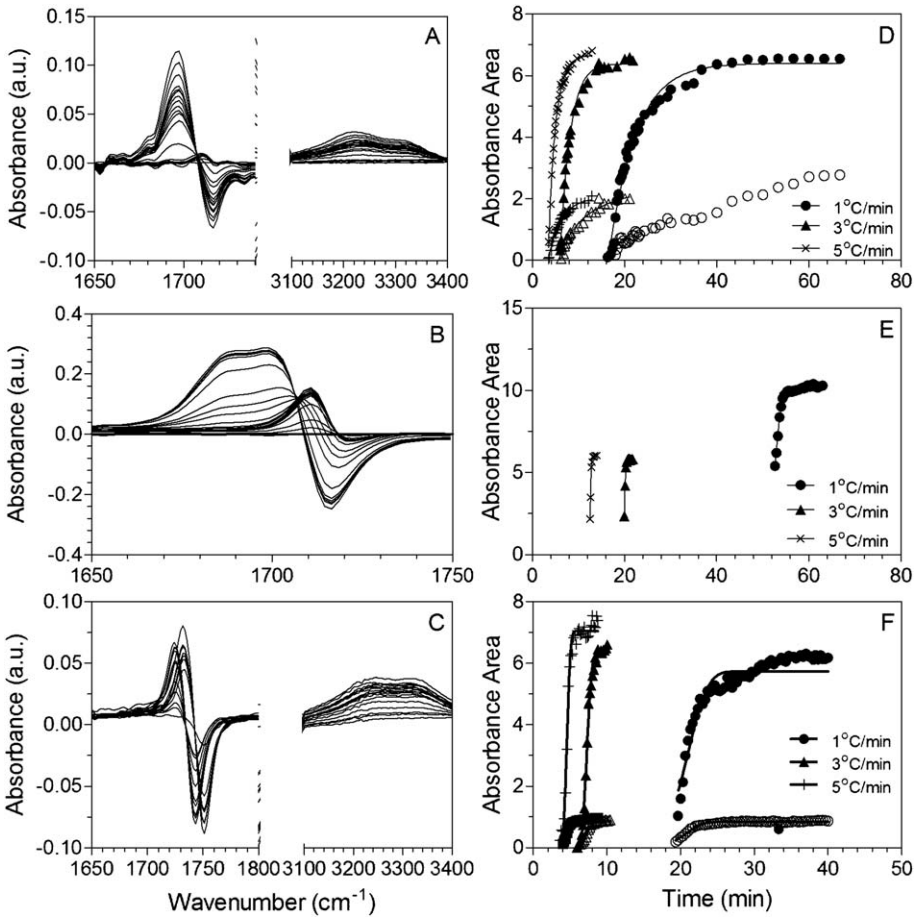

Fig. 2 A sampling of FT-IR spectra of 12HSA (A), stearic acid (B) and trihydroxystearin (C) cooled at 1 °C min^{-1} from 90 °C to 30 °C and their respective area under the peak plotted over time fitted to the modified Avrami model (D, E, and F respectively). The filled and open symbols in data points for (D) and (F) represent the carboxyl peak (1710 cm^{-1}) and hydroxyl peak (3200 cm^{-1}) respectively.

peak associated with crystallization. The onset of crystallization was determined by the observable inflection point on the collected thermograms. From the inflection point, the thermogram was integrated till no significant change was observed between data points. The obtained integrated curve followed a sigmoidal line indicative of a crystallization event and was fitted to the modified Avrami model. Three replicates were performed for this analysis to obtain statistical significance.

Small deformation rheology

An AR1000 rheometer with a 4 cm diameter flat stainless steel parallel plate geometry monitored the evolution of the storage modulus (G') (TA Instruments, New Castle, Delaware, USA). Approximately 1.26 mL of the melted sample was held by the rheometer between the Peltier plate and the geometry. The sample thickness was controlled by the rheometer and held at 1000 μm. The measurements were conducted using a 10 Pa oscillatory stress and a frequency of 1 Hz as it was cooled from 90 °C to 30 °C. 10 Pa was selected as the ideal oscillatory stress as it was the lowest value obtained from the linear viscoelastic region in the solid state for all the samples. The modified Avrami model was fitted to the evolving G'. Three replicates were performed for this analysis to obtain statistical significance.

Polarized light microscopy

A Nikon Eclipse E400 light microscope equipped with a Nikon DS-FiL color camera and a long working distance 10× lens and condenser (Nikon Instruments Inc., Melville, NY, USA) was used to acquire polarized light micrographs. A temperature controlled stage (LTS120 and PE94 temperature controller (Linkam, Surrey, UK)) was used to control the cooling rates. The image resolution was 2560 by 1920 pixels. Images were analyzed using Adobe Photoshop Extended CS4.0 (Adobe Systems Incorporate, San Jose, CA, USA) to determine the length of the crystals. Sample preparation consists of taking a drop of the melted sample and spreading it onto a glass microscopy slide. Micrographs were taken as the sample cooled and the average of 10 crystals was taken to represent the average length at a given time. The growth of the average crystal length was measured as a function of time for each cooling rate. Three replicates were obtained to ensure statistical significance.

Fitting the modified Avrami model

Fitting the data was done using Graphpad Prism 5.0 (www.graphpad.com, La Jolla, CA) where initial values of Y_{max}, k_{app}, x_o and n were given and the software determined the best fit values through an iterative process (1000 iterations). None of the terms were confined during the iterative process. The initial Y_{max}

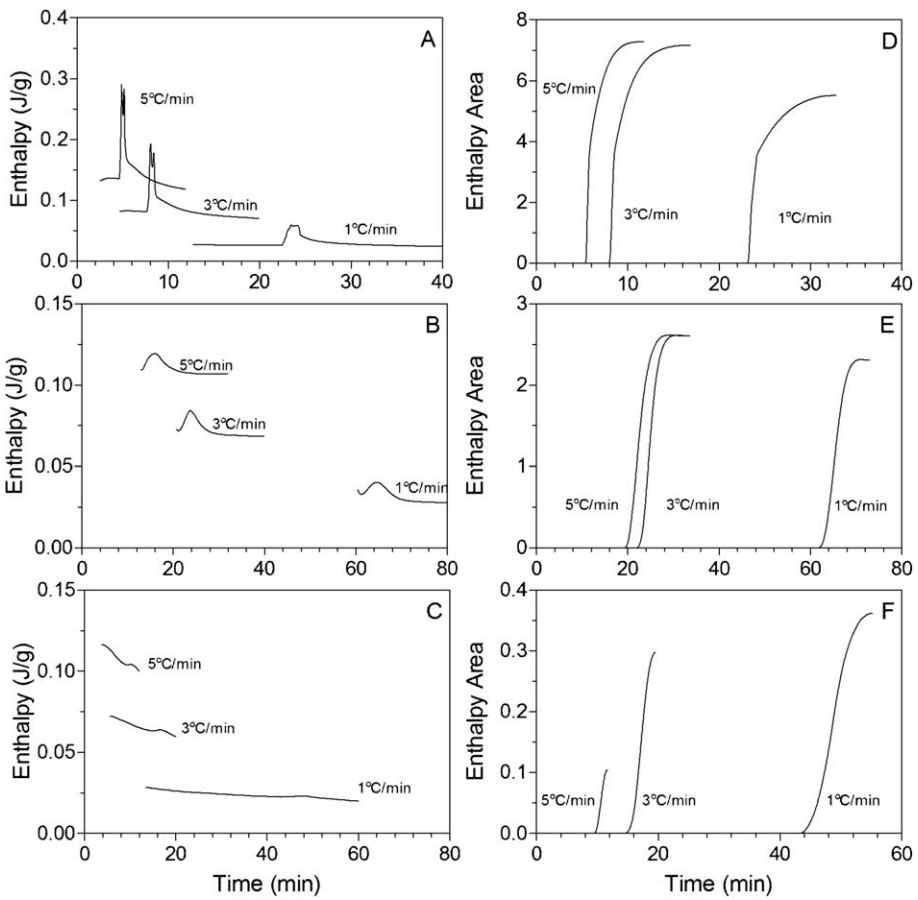

Fig. 3 A sampling of DSC thermograms of 12HSA (A), stearic acid (B) and trihydroxystearin (C) cooled at different rates and a plot of their respective continuous integration for the different cooling rates fitted to the modified Avrami model (D–F respectively).

used was the maximum signal detected. The exponent n was initially set to 1, 2, or 3 for 12HSA, stearic acid and trihydroxystearin; respectively. Finally, k_{app} and x_0 were set to zero and determined by the software.

Results and discussion

Carboxylic acid dimerization is observed by the increase in the peak area at 1710 cm^{-1} and a simultaneous decrease at 1700 cm^{-1} corresponding to the stretching of the free carboxylic acid monomer.[35] Dimerization of the free carboxylic acid groups and the hydrogen bonding of the hydroxyl group at position 12 on the fatty acid may be monitored using FT-IR for 12HSA (Fig. 2A). Stearic acid crystallization was monitored by the dimerization of the carboxylic acid monomers (Fig. 2B). Trihydroxystearin crystallization was monitored by the 3200 cm^{-1} peak corresponding to the hydrogen bonding at the 12 carbon position on the fatty acid (Fig. 2C). The areas of these peaks have previously been correlated to the formation of non-covalent intermolecular interactions in the crystalline phase and have been used to quantify the amount crystalline material.[36,37] Since FT-IR has been used to measure the phase volume it is an ideal method to fit the modified Avrami model too. The CH_2 stretching was detected, however, it was not possible to differentiate changes for the crystalline phase from the mineral oil. Therefore no analysis could be complied on the CH_2 groups in the sample. The FT-IR signals (Fig. 2A–C) were integrated and the area under the curve was plotted as a function of time and fitted to the modified Avrami model (Fig. 2D–F) obtaining the Avrami exponent, induction time and maximum phase change.

DSC is commonly used to measure the heat released during exothermic crystallization events.[23,25,38–42] A single enthalpy peak was observed for each of the gelator molecules during crystallization and the peak (Fig. 3A–C) was integrated using a running integral which was then fitted to the modified Avrami model (Fig. 3D–F). The use of the running integral to represent the crystallization process in DSC has been previously reported and the data collected were fitted to the modified Avrami model (Fig. 3D–F).[23]

The presence of network formation was monitored through the storage modulus (G') (Fig. 4). Although the plot gave the typical sigmoidal shaped curve which the Avrami equation is typically used to model; G' is not a measure of the phase volume of the new phase. The storage modulus or the elastic component of the material is a function in part of the solid content but also is

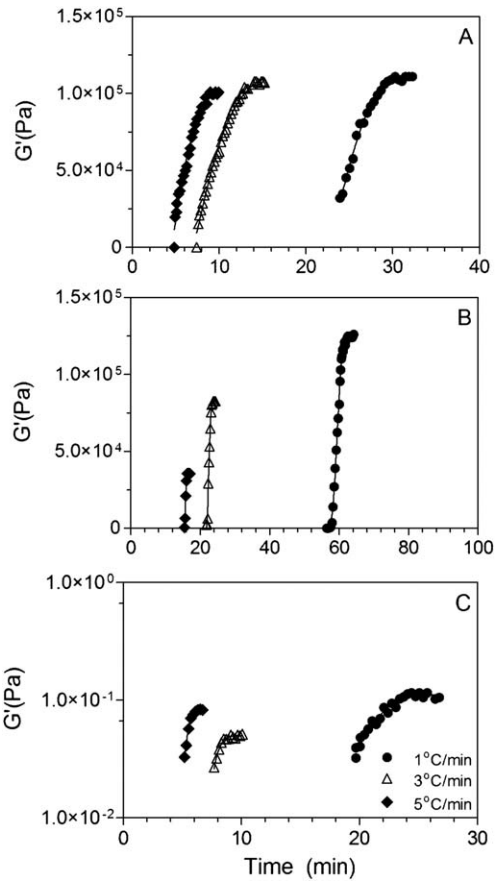

Fig. 4 A sampling of the storage modulus obtained for 12HSA (A), stearic acid (B) and trihydroxystearin (C) collected under different cooling rates and fitted to the modified Avrami model.

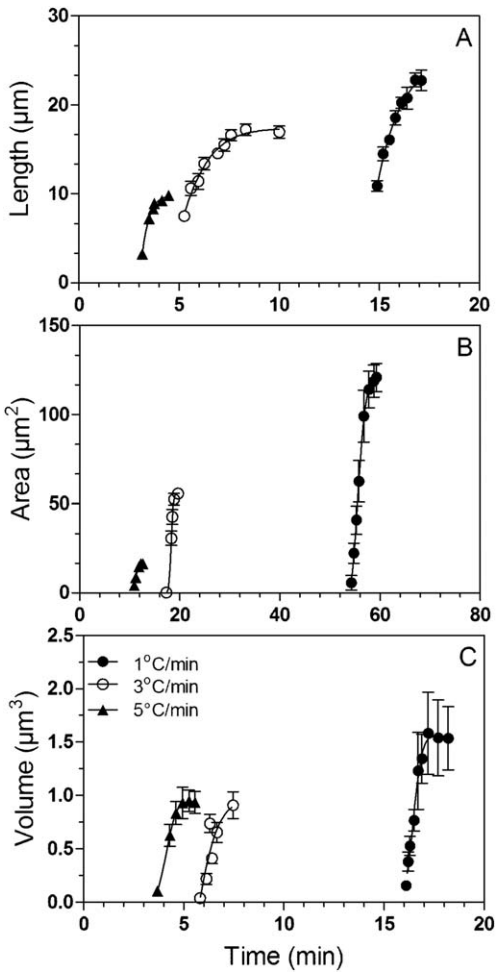

Fig. 5 A sampling of PLM characteristic lengths corrected for their dimensionality of crystal growth for 12HSA 1-D fibers (A), stearic acid 2-D platelets (B) and trihydroxystearin 3-D spheres (C) and fitted to the modified Avrami model.

a function of the spatial distribution of mass, crystal shape and entanglement of the new phase.

Finally, PLM visualizes birefringent anisotropic crystals. Birefringence is the double refraction of light through an anisotropic material.[43] PLM allows for the visualization of crystal microstructure where birefringent anisotropic crystals appear bright while the liquid oil remains dark under polarized light.[43] Under PLM, 12HSA appears as long helical fibers which are observed as a segmented line representing the crystals being in and out of phase with the cross-polarizers (Fig. 1A).[5,7,20,44–47] Stearic acid crystals are rhombic shaped[32,33,48] (Fig. 1B) and trihydroxystearin appears as Maltese crosses (Fig. 1C). Spherical growth is often identified by the presence of the Maltese cross under polarized light.[49–51] For 12HSA, the length of the fiber was recorded. For stearic acid, the maximum length of the rhombic crystal was recorded and the radius of trihydroxystearin spherulite crystal was determined. However, the measurement must be converted to a measure of the phase volume prior to fitting the data to the modified Avrami model. The fiber length is characteristic of the phase volume in one dimensional growth. For the two and three dimensional samples, the measurement of the maximum length in a crystal is not representative of their respected dimensionalities. The phase volume for platelets was approximated by calculating the area of the platelet and squaring the length, while for trihydroxystearin phase volume was determined cubing the radius to determine the area for a sphere. The crystal phase volume was plotted as a function of time and fitted to the modified Avrami model (Fig. 5).

A sigmoidal crystal growth curve was found for each sample, cooling rate and technique measured (Fig. 2–5). The Avrami exponents obtained from the fits to the modified Avrami model are presented in Fig. 6. Fig. 6 indicates that the model accurately predicted the correct dimensionality of growth using DSC (Fig. 6C, G and K) and PLM (Fig. 6B, F and J). While for FT-IR (Fig. 6A, E and I) the correct dimensionality of crystal growth and mode of nucleation were predicted. Sporadic nucleation occurred at slow cooling and instantaneous nucleation at faster cooling rates which are congruent to general principles of crystallization. At low degrees of supercooling (*i.e.*, low cooling rates) the activation energy for nucleation is harder to overcome leading to greater ease of crystal growth than nucelation.[4] At high degrees of supercooling, the activation energy is easier to overcome and nucleation is favored over crystal growth which leads to a high nucleation rate and smaller crystals.[4]

Fractional Avrami exponents were observed when the storage modulus, determined using rheology, was fitted to the modified Avrami model (Fig. 6D, H and L). It is possible that the fractional Avrami exponents may be due to the contraction of the material during cooling which affects the G' obtained. A true-gap system has been shown to improve rheological results during crystallization as it accounts for the contraction of the material.[52] The storage modulus is not only a function of the change in phase volume but also the spatial distribution of mass, crystal size and inter-crystal interactions.[53] Therefore, the measure of the system is not purely a measure of the change in phase volume.[14,53] The dimensionality of crystal growth from the Avrami exponents was also verified by the PLM micrographs taken when the sample reached the final temperature (Fig. 1). The model was capable of determining the correct dimensionality of growth using DSC and PLM but the mode of nucleation was only detected under FT-IR.

The calculated induction times were compared for each method, cooling rate and sample (Fig. 7). A comparison of the experimentally observed *versus* the calculated induction times was found to have less than 5% difference (data not presented). The induction time dictates whether a method can detect the onset of nucleation. The observed induction times were

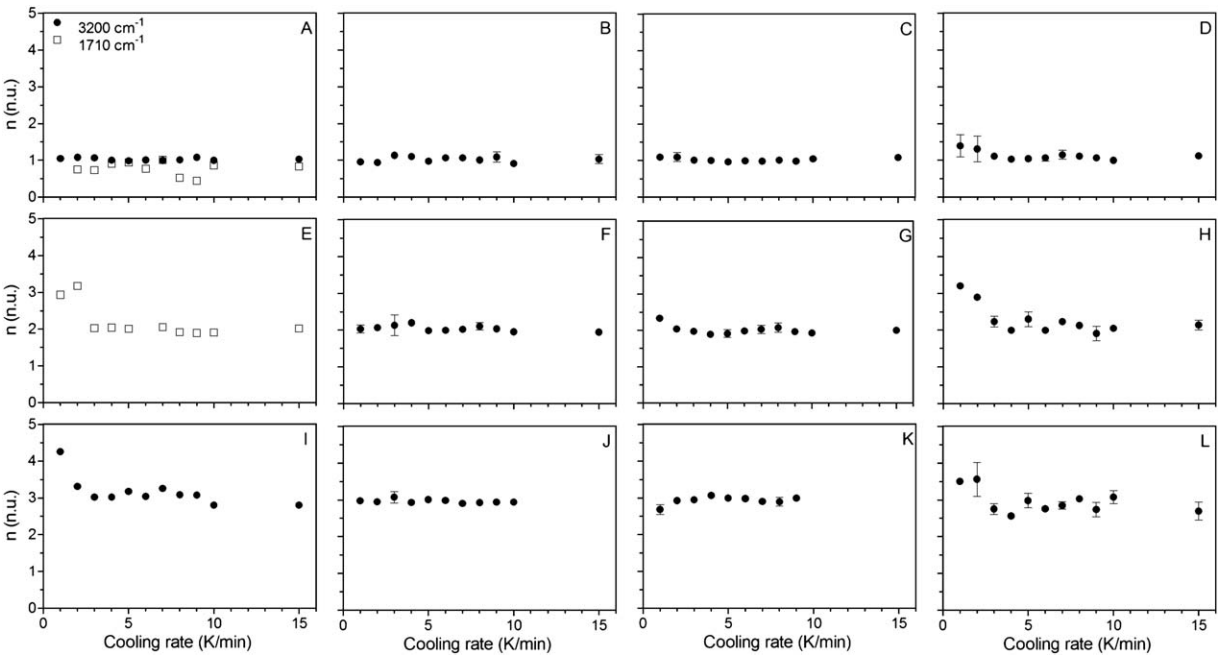

Fig. 6 Avrami exponents (n) calculated from the fits of the experimentally observed data to the modified Avrami model for FT-IR (A, E and I), PLM (B, F, and J), DSC (C, G, and K) and rheology (D, H and L) for 12HSA (A–D), stearic acid (E–H) and trihydroxystearin (I–L).

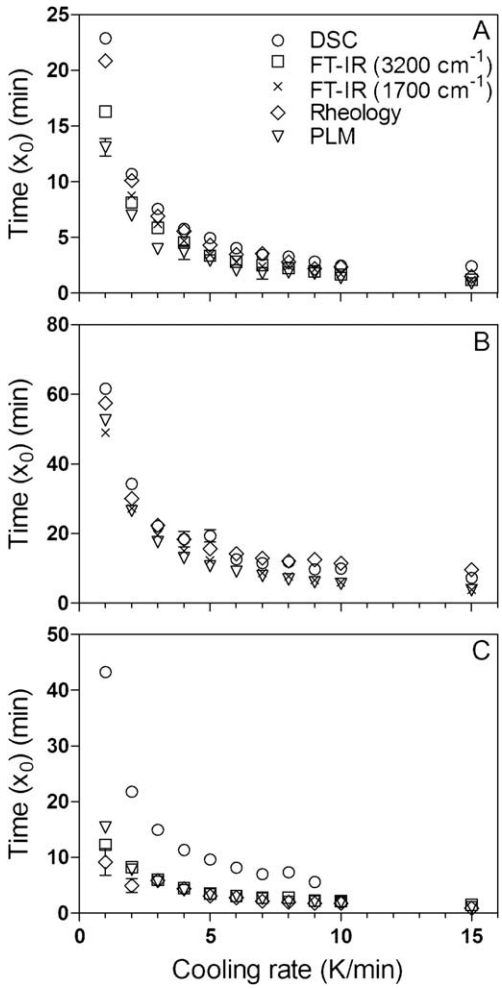

Fig. 7 The induction times (x_0) of the fitted data for 12HSA (A), stearic acid (B) and trihydroxystearin (C).

determined by the inflection point on the graphs for FT-IR, DSC and rheology. In FT-IR, the inflection point was determined based on the plot of the absorbance area over time. The inflection point for DSC was determined by the change in the integrated curve over time whereas in rheology it was based on the change in the storage modulus. For PLM, the observed induction time was based on the initial presence of nuclei observed under polarized light. The fitted induction times were determined using the modified Avrami model. At low cooling rates, the earliest induction time was detected by PLM and FT-IR while rheology and DSC occurred significantly later (Fig. 7).

The induction time, determined using DSC, has a delayed onset due to the thermodynamics of nucleation which is a complex relationship between the decrease in entropy and release of enthalpy during nuclei formation.[54] At the early stages of crystallization, the heat released from the formation of the first few nuclei may not be captured by DSC.[55] Therefore it is difficult to determine an accurate induction time. Rheology measures the elastic properties of the network which occur upon the formation of a continuous network significantly later than the onset of nucleation.[56,57] In trihydroxystearin and stearic acid, entanglement of the network does not occur as readily as 12HSA and hence a significantly lower G' is observed. Both PLM and FT-IR determined the dimensionality of crystal growth while only FT-IR appeared to be sensitive to the mode of nucleation. Therefore the modified Avrami model is capable of not only determining the dimensionality of crystal growth but also the induction time.

The maximal signal, or maximum phase volume (Y_{max}), is also an important parameter in the modified Avrami model. While the induction time indicates when the first sign of the crystallization event is detected, Y_{max} indicates when the phase volume has reached its maximum at that given temperature. The observed Y_{max} *versus* the calculated Y_{max} was plotted for the different samples and cooling rates were plotted (Fig. 8). The Y_{max} values obtained for the observed overlapped those that were calculated (Fig. 8). This indicates that the model was capable of correctly fitting to the maximal measured change in the phase volume (Y_{max}). Though the maximal change in phase volume (Fig. 8) and induction times (Fig. 7) for the experimentally observed values correlated well with the fitted values, not all four of the methods used predicted good parameters for the modified Avrami model. In order to obtain an accurate Avrami exponent and rate constant, the method must detect the early formation of nuclei. The inability for DSC to detect the heat released at early stages of crystallization leading to a delayed induction time invalidates it as a candidate to predict accurate rate constants. Though rheology also obtained a later induction time than other techniques (Fig. 7), it was able to detect the transition prior to DSC. Rheology obtained a later induction time (Fig. 7) and predicted fractional Avrami exponents which were not observed in the other methods (Fig. 6D, H and L). For the aforementioned reasons, the data obtained by FT-IR and PLM were considered valid and further insights were gained into the apparent rate constants (k_{app}).

The apparent rate constants, k_{app}, were determined by fitting the data to the modified Avrami model (Fig. 9). Under isothermal cooling conditions, as the crystallization temperature decreases, the crystallization rate constant increases.[14–16] Therefore, under non-isothermal crystallization conditions it is expected that the rate constant will increase as the cooling rate increases. Furthermore, when comparing the rate constants obtained by the two methods, an increase in cooling rate is accompanied by the increase in rate constant until it plateaus at higher cooling rates (Fig. 9). This phenomenon may be explained by the two components of the rate constant: diffusion and reaction rates.[4] Diffusion limited reactions occur when the crystallization rate is limited by the molecules ability to diffuse to the crystal surface; while, reaction limited crystallization occurs when the rate of incorporation of the molecule into the crystal lattice is limited.[4] A dual trend was observed for the apparent rate constants (k_{app}) obtained below and above the cooling rates of 5–7 °C min^{-1}. A steeper slope was observed among the lower regime of cooling rates whereas a shallower slope was observed for the upper regime. This dual trend observation is congruent with observations made by previously reported research.[17,18] Slow cooling profiles lead to crystallization being diffusion limited while at faster cooling rates crystallization is reaction limited.[23] A similar result was previously reported in non-isothermal cooling conditions for crystallization using the isoconversional technique.[23] Under low cooling rates, the thermodynamic driving force for crystallization is low allowing

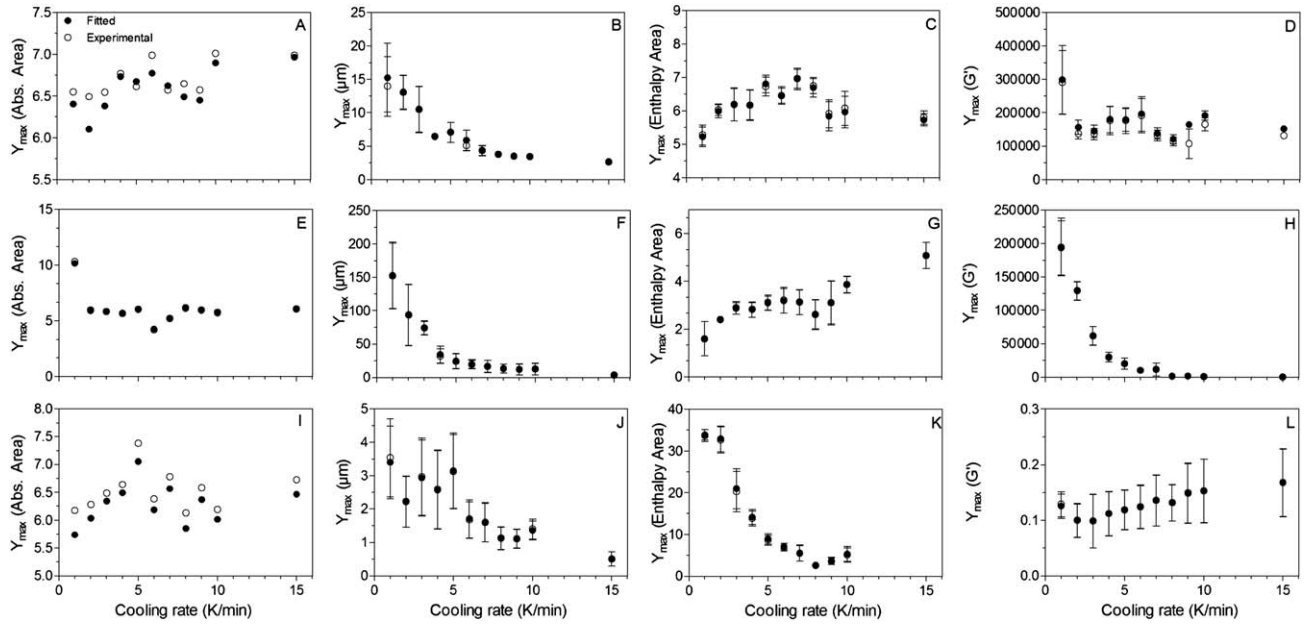

Fig. 8 The maximal measure of the change in the phase volume (Y_{max}) as a function of cooling rate for the experimentally observed *versus* the fitted data to the modified Avrami model for FT-IR (A, E and I), PLM (B, F, and J), DSC (C, G, and K) and rheology (D, H and L) for 12HSA (A–D), stearic acid (E–H) and trihydroxystearin (I–L).

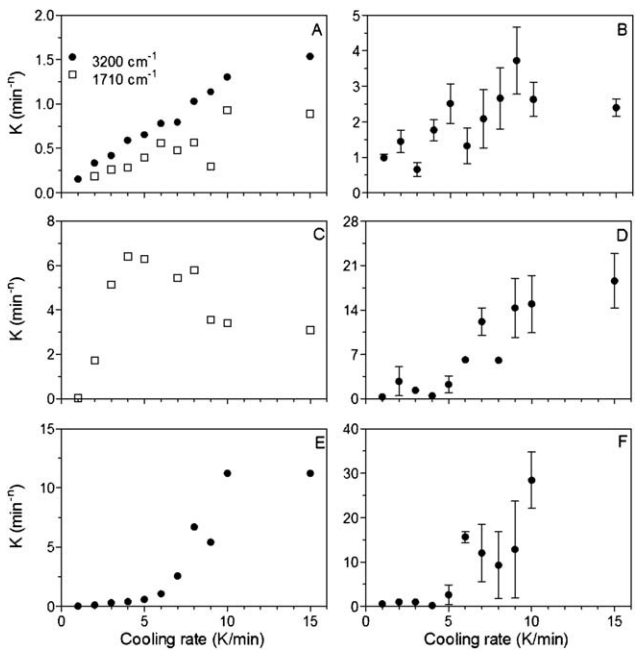

Fig. 9 Apparent rate constants (k_{app}) obtained from the experimental fits of the data to the modified Avrami model for FT-IR (A, C, and E) and PLM (B, D, and F) for 12HSA (A and B), stearic acid (C and D) and trihydroxystearin (E and F).

molecules near or at the crystal–solvent interface to orient before incorporating into the crystal lattice.[4,53] Under high cooling rates, the thermodynamic driving force is high and the molecules do not have the time to attain the optimal configuration before incorporation into the crystal lattice.[4,53] This yields imperfectly formed crystals which were previously reported in the crystallization of 12HSA as branched fibers.[53]

Conclusions

The application of the modified Avrami model requires the data to be a measure only of the change in phase volume. When this criterion is not met, fractional Avrami exponents were obtained, invalidating the data. The experimental validation of the modified Avrami model relies on the model to accurately predict the Avrami exponent (n), induction time (x_0) and the maximal signal (Y_{max}). For all the data collected, the experimentally observed maximal signal (Y_{max}) and the induction time (x_0) corresponded well with the fitted parameters. An accurate Avrami exponent (n) requires that the experimental method capable of detecting early nucleation events. Both the PLM and FT-IR reported early induction times (x_0). Furthermore, FT-IR was the only method to determine the mode of nucleation with the dimensionality of crystal growth. This suggests that the FT-IR method is the most accurate method to characterize the non-isothermal crystallization of materials providing significant insights into the apparent rate constant (k_{app}).

Acknowledgements

The work presented here was funded by NSERC. The research described in this paper was preformed, in part, at the Canadian Light Source, which is supported by NSERC, NRC, CIRH and the University of Saskatchewan. The authors wish to thank Tim May and Tor Pederson for their help, upkeep and maintenance of the Mid-IR Beamline at the Canadian Light Source (Saskatoon, SK, Canada).

References

1 J. T. Hu, T. W. Odom and C. M. Lieber, *Acc. Chem. Res.*, 1999, **32**, 435–445.

2 B. T. Holland, C. F. Blanford, T. Do and A. Stein, *Chem. Mater.*, 1999, **11**, 795–805.
3 B. J. Wang, C. Y. Li, J. Hanzlicek, S. Z. D. Cheng, P. H. Geil, J. Grebowicz and R. M. Ho, *Polymer*, 2001, **42**, 7171–7180.
4 A. G. Marangoni, in *Fat Crystal Networks*, ed. A. G. Marangoni, Marcel Dekker, New York, 2005, pp. 21–82.
5 M. A. Rogers, *Food Res. Int.*, 2009, **42**, 747–753.
6 M. A. Rogers, A. J. Wright and A. G. Marangoni, *Soft Matter*, 2009, **5**, 1594–1596.
7 M. A. Rogers, A. J. Wright and A. G. Marangoni, *Curr. Opin. Colloid Interface Sci.*, 2009, **14**, 33–42.
8 A. Bot and W. G. M. Agterof, *J. Am. Oil Chem. Soc.*, 2006, **83**, 513–521.
9 F. G. Gandolfo, A. Bot and E. Floter, *J. Am. Oil Chem. Soc.*, 2004, **81**, 1–6.
10 D. Li and Y. N. Xia, *Nano Lett.*, 2004, **4**, 933–938.
11 K. Hanabusa, T. Miki, Y. Taguchi, T. Koyama and H. Shirai, *J. Chem. Soc., Chem. Commun.*, 1993, 1382–1384.
12 J. Jin, M. Song and F. Pan, *Thermochim. Acta*, 2007, **456**, 25–31.
13 R. G. Weiss and P. Terech, in *Molecular Gels: Materials with Self-Assembled Fibrillar Networks*, ed. R. G. Weiss and P. Terech, Springer, Dordrecht, 2006, pp. 1–13.
14 M. Avrami, *J. Chem. Phys.*, 1939, **7**, 1103.
15 M. Avrami, *J. Chem. Phys.*, 1940, **8**, 212.
16 M. Avrami, *J. Chem. Phys.*, 1941, **9**, 177.
17 M. A. Rogers and A. G. Marangoni, *Cryst. Growth Des.*, 2008, **8**, 4596–4601.
18 M. A. Rogers and A. G. Marangoni, *Langmuir*, 2009, **25**, 8556–8566.
19 A. G. Marangoni and S. E. McGauley, *Cryst. Growth Des.*, 2003, **3**, 95–108.
20 M. A. Rogers, A. J. Wright and A. G. Marangoni, *Soft Matter*, 2008, **4**, 1483–1490.
21 A. Sharples, *Introduction to Polymer Crystallization*, Edward Arnold, Ltd., London, 1966.
22 A. G. Marangoni, *J. Am. Oil Chem. Soc.*, 1998, **75**, 1465–1467.
23 L. Bouzidi and S. S. Narine, *Langmuir*, 2010, **26**, 4311–4319.
24 P. Rousset, in *Physical Properties of Lipids*, ed. A. G. Marangoni and S. S. Narine, Marcel Dekker, New York, 2002, pp. 1–36.
25 K. W. Smith, F. W. Cain and G. Talbot, *J. Agric. Food Chem.*, 2005, **53**, 3031–3040.
26 P. Terech and R. G. Weiss, *Chem. Rev.*, 1997, **97**, 3133–3160.
27 X. Huang and R. G. Weiss, *Tetrahedron*, 2007, **63**, 7375–7385.
28 V. A. Mallia, M. George, D. L. Blair and R. G. Weiss, *Langmuir*, 2009, **25**, 8615–8625.
29 Z. Huo, S. Dai, C. Zhang, F. Kong, X. Fang, L. Guo, W. Liu, L. Hu, X. Pan and K. Wang, *J. Phys. Chem. B*, 2008, **112**, 12927–12933.
30 J.-L. Li, R.-Y. Wang, X.-Y. Liu and H.-H. Pan, *J. Phys. Chem. B*, 2009, **113**, 5011–5015.
31 M. Suzuki, Y. Nakajima, M. Yumoto, M. Kimura, H. Shirai and K. Hanabusa, *Langmuir*, 2003, **19**, 8622–8624.
32 H. M. Schaink, K. F. van Malssen, S. Morgado-Alves, D. Kalnin and E. van der Linden, *Food Res. Int.*, 2007, **40**, 1185–1193.
33 R. S. N. Swamy, P. B. V. Prasad and I. Raju, *Cryst. Res. Technol.*, 1985, **20**, 803–807.
34 A. G. Marangoni, in *Fat Crystal Networks*, ed. A. G. Marangoni, Marcel Dekker, New York, 2005, pp. 1–20.
35 D. Lin-Vien, N. B. Colthup, W. G. Fateley and H. G. Grasselli, *The Handbook of Infrared and Raman Characteristic Frequencies of Organic Molecules*, Academic Press, New York, 1991.
36 J. Cornel and M. Mazzotti, *Ind. Eng. Chem. Res.*, 2009, **48**, 10740–10745.
37 H. Huang, L. X. Gu and Y. Ozaki, *Polymer*, 2006, **47**, 3935–3945.
38 M. A. Grompone, R. Correa-Cabrera and B. Irigaray, *Ing. Quim. (Madrid, Spain)*, 1999, **16**, 45–55.
39 K. Chaleepa, A. Szepes and J. Ulrich, *Chem. Phys. Lipids*, 2010, **163**, 390–396.
40 R. Campos, M. Ollivon and A. G. Marangoni, *Cryst. Growth Des.*, 2010, **10**, 205–217.
41 L. Ahmadi, A. J. Wright and A. G. Marangoni, *Eur. J. Lipid Sci. Technol.*, 2008, **110**, 1014–1024.
42 K. Sato, *Chem. Eng. Sci.*, 2001, **56**, 2255–2265.
43 R. Campos, in *Fat Crystal Networks*, ed. A. G. Marangoni, Marcel Dekker, New York, 2005, pp. 267–348.
44 J. H. Fuhrhop, P. Schnieder, J. Rosenberg and E. Boekema, *J. Am. Chem. Soc.*, 1987, **109**, 3387–3390.
45 T. Tachiban and H. Kambara, *J. Colloid Interface Sci.*, 1968, **28**, 173–174.
46 P. Terech, V. Rodriguez, J. D. Barnes and G. B. McKenna, *Langmuir*, 1994, **10**, 3406–3418.
47 Y. Uzu and T. Sugiura, *J. Colloid Interface Sci.*, 1975, **51**, 346–349.
48 F. Gandolfo, A. Bot and E. Flöter, *J. Am. Oil Chem. Soc.*, 2004, **81**, 1–6.
49 K. G. Berger, G. G. Jewell and R. J. M. Pollitt, in *Food Microscopy*, ed. J. G. Vaughan, Academic Press, London, 1979, pp. 445–497.
50 L. A. Gioielli, I. S. Simoes and J. N. Rodrigues, *J. Food Eng.*, 2003, **57**, 347–355.
51 M. L. Meara, in *Fats and Oils: Chemistry and Technology*, ed. R. J. Hamilton and A. Bhati, Applied Science, London, 1980, pp. 193–213.
52 J. A. Morales-Rueda, E. Dibildox-Alvarado, M. A. Charo-Alonso and J. F. Toro-Vazquez, *J. Am. Oil Chem. Soc.*, 2009, **86**, 765–772.
53 R. Lam, L. Quaroni, T. Pederson and M. A. Rogers, *Soft Matter*, 2010, **6**, 404–408.
54 P. Walstra, *Physical Chemistry of Foods*, Marcel Dekker, Inc., New York, 2003.
55 E. Piorkowska, A. Galeski and J. M. Haudin, *Prog. Polym. Sci.*, 2006, **31**, 549–575.
56 C. Schwittay, M. Mours and H. H. Winter, *Faraday Discuss.*, 1995, **101**, 93–104.
57 H. H. Winter, *Korea Aust. Rheol. J.*, 1999, **11**, 275–278.